Aplite diking and infiltration: a differentiation mechanism restricted to plutonic rocks

Allen F. Glazner[1] · John M. Bartley[2] · Drew S. Coleman[1] · Kjell Lindgren[3]

Received: 19 June 2019 / Accepted: 16 March 2020 / Published online: 1 April 2020

Abstract
The Half Dome Granodiorite in Yosemite National Park, California, contains multiple crosscutting generations of high-silica dikes that vary in texture but share the distinctive trace element characteristics of fine-grained aplite dikes of the region (e.g., low Y and middle REE). Dikes of the youngest generation are typical fine-grained, sugary aplites with sharp planar contacts, whereas progressively older dikes are increasingly coarse-grained. The oldest ghostly forms recognizable as dikes are similar in grain size to the host granodiorite and their contacts are irregular at the grain scale, making them easy to overlook in the field. Mineral compositions and microstructures of felsic dikes indicate that all dikes, including fine-grained aplite, have undergone significant recrystallization. We propose that older dikes were originally fine-grained aplites that, after emplacement, recrystallized together with the host to a typical granitic texture. Extraction, transport, and redistribution of aplitic melt by various mechanisms explains major and trace element variation in the pluton and likely was the dominant differentiation mechanism at the level of emplacement. This late-stage differentiation process can only occur in a largely crystallized host capable of sustaining tensile cracks, and therefore cannot play a role in the differentiation of volcanic rocks. Predicted geochemical effects of aplite redistribution are evident in trace-element geochemical patterns of Circum-Pacific plutonic rocks but are absent from corresponding volcanic rocks. This indicates that aplite infiltration may be an important and widespread late-stage process of pluton differentiation.

Keywords Granite · Differentiation · Geochemistry · Recrystallization

Introduction

Origins of geochemical variability in plutons

The origin of geochemical variability in igneous rocks—in particular, how the compositional spectrum from basalt to rhyolite is produced—has been a focus of igneous petrology research for more than a century. Although there is little consensus, some combination of crystal–liquid separation, magma mixing, and partial melting is generally called upon to explain the overall compositional variability of igneous systems (e.g., Bowen 1928; Blake et al. 1965; Michael 1984; Sisson et al. 2005; Grove and Brown 2018).

Here, we focus on petrological variations displayed by the Tuolumne Intrusive Suite (TIS), an archetypal large nested plutonic suite of the Cretaceous Sierra Nevada batholith of California (Bateman 1992). The TIS is zoned from outer mafic granodiorite and tonalite, through a dominant volume of granodiorite, to a small body of leucogranite that makes up its core (Bateman et al. 1983), with individual plutonic units mapped based on the texture. SiO_2 ranges from ~ 59 to 75 wt%, and intrusion of the entire suite took on the order of 10 Ma, between about 95 and 85 Ma (Coleman et al. 2004). These geochronologic data have been interpreted to indicate assembly of the TIS from myriad small batches (Coleman et al. 2004, 2012; Glazner et al. 2004; Gray et al. 2008; Bartley et al. 2018); if true, then traditional differentiation processes that require a large upper-crustal magma chamber

Communicated by Othmar Müntener.

✉ Allen F. Glazner
afg@unc.edu

[1] Department of Geological Sciences, University of North Carolina, Chapel Hill, NC 27599-3315, USA

[2] Department of Geology and Geophysics, University of Utah, Salt Lake City, UT 84112-1183, USA

[3] Astronaut Office, Mail Code CB, National Aeronautics and Space Administration-Johnson Space Center, 2101 NASA Parkway, Houston, TX 77058, USA

(e.g., Bateman and Chappell 1979; Memeti et al. 2010) did not operate. This further implies that first-order petrologic variations in the TIS, i.e., those between major plutonic units, were produced in the magma source and/or during ascent rather than at the emplacement level. However, field, petrographic, and geochemical evidence suggests that ascent of aplitic pore melt through a largely static crystalline matrix by a combination of porous flow and diking caused late-stage differentiation at the level of emplacement.

Previous work

This study focuses on felsic dikes in the Half Dome Granodiorite (Fig. 1), which was emplaced between 93 and 89 Ma, midway through assembly of the TIS. Coleman et al. (2012) and Bartley et al. (2018) mapped and characterized the geochemistry of cyclical compositional variations on length scales ranging from several km down to meter-scale in this unit. Because these results form the framework for the present study, we briefly summarize them here.

Coleman et al. (2012) studied lithologic variability in the Half Dome Granodiorite using standard field mapping augmented with nearly 1500 magnetic susceptibility stations. Within the western lobe of the granodiorite, they found seven km-scale lithologic cycles, each of which is bounded by a sharp west-dipping contact that is subparallel to the external contact of the pluton. Crosscutting relations indicate that the cycles become younger to the east. They interpreted each cycle to have been a zone of interconnected melt in which an eastern melt-depleted base grades westward to a melt-rich top now preserved as a leucocratic facies of the Half Dome Granodiorite. Sharp contacts between cycles may record freezing episodes when the rate of heat input into the growing pluton dropped below that required to maintain interstitial melt. These cycles occur on the outer, older margins of the suite, and disappear toward the interior, younger intrusions. Inward disappearance of cycles is interpreted to reflect thermal maturation of the system such that melt was continuously present until magmatic input ceased and the system froze.

Although the cycles span the compositional range from mafic granodiorite to leucogranite, trace element trends preserved in the cycles differ dramatically from those of both the Tuolumne Intrusive Suite and other Cretaceous zoned plutons of the eastern Sierra Nevada batholith. Coleman et al. (2012) proposed that the overall compositional variations between various plutonic units in the batholith reflect a signal from the source of the magmas, but that geochemical variations within the km-scale cycles reflect in situ crystal/liquid separation.

Bartley et al. (2018) took advantage of nearly 100% exposure on glacially polished slabs to map the meter-scale internal structure of the mafic-to-felsic transition within one of

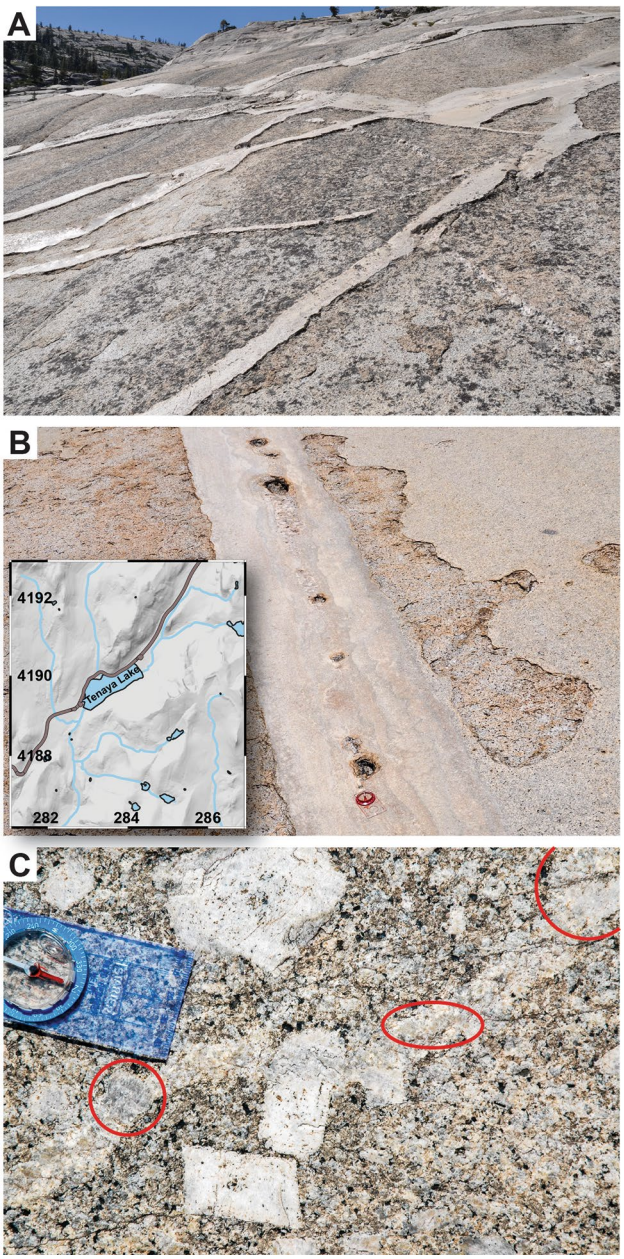

Fig. 1 Aplite and leucogranite dikes near Tenaya Lake, Yosemite National Park, California. Inset map shows location of study area, surrounding Tenaya Lake; margins give UTM coordinates in km, zone 11 N. **a** Polished dikes standing out in relief on formerly polished section of granodiorite; many more dikes are visible in weathered surfaces adjacent to obvious dikes. Dike in foreground is ~ 30 cm wide. **b** Layered leucogranite dike with pegmatite and numerous hydrothermal pipes in its core. Compass circle is 5 cm in diameter. Glacial polish is largely absent left of the dike and mostly preserved to the right. See Fournier (1968). **c** A coarse-grained leucogranite dike 1–2 cm thick cuts a K-feldspar megacryst that has partially healed across the fracture. Nearby crystals cut by similar dikes have completely healed (Glazner and Johnson 2013, their Fig. 13a). The dike contains numerous crystals 1–2 cm across, including a particularly large K-feldspar just below the right edge of the compass. Compass circle is 5 cm in diameter

the kilometer-scale cycles. This revealed an intricate plexus of crosscutting and variably deformed dikes. Fournier (1968) mapped a similar plexus of dikes in a nearby area, and observations presented in this paper come from both map areas. The bodies are interpreted to be dikes based on tabular shape, contacts with surrounding granodiorite that truncate markers (e.g., mafic enclaves, K-feldspar megacrysts, older dikes) which commonly can be matched across the dike, and geometrical features typical of crack systems such as branches, jogs, relays, and T-intersections. Note that use of the term "dike" here only refers to injection of magma into a dilating crack and carries no connotation regarding orientation.

Three-dimensional exposures are extremely limited on the slabs but, where measurable, dikes dip broadly toward the west from 30° to 70°. The dikes are predominantly felsic but modal layering on a scale of 0.1–1 m is common, with a thin mafic base grading upward into leucogranite that forms the majority of the dike. Compositions and textures of mapped dikes form a continuum ranging from coarse-grained with abundant mafic–felsic layering to fine-grained aplite. Mapped dikes range in thickness from roughly 10 cm to 10 m. Layered dikes thicker than 1 m invariably contain multiple mafic–felsic cycles, and crosscutting relations indicate that each mafic–felsic cycle represents a distinct incremental addition. Syn-intrusive deformation is recorded by folding of earlier dikes that are crosscut by dikes that are undeformed. The field relations thus indicate a complex and protracted history of dike injection during the assembly of each kilometer-scale compositional cycle. This paper further explores the processes that link meter-scale and kilometer-scale variations in the Half Dome Granodiorite and their implications for differentiation.

Methods

We examined glacially polished slabs in two areas of exceptional exposure and high leucocratic dike abundance within the Half Dome Granodiorite near Tenaya Lake in Yosemite National Park (Fig. 1). Glacial polish is widespread, covering anywhere from 50% to nearly 100% of hectare-sized areas. The rocks are exposed mostly on smoothly curving polished surfaces that offer near-perfect two-dimensional exposure but few sampling opportunities. National Park Service regulations prohibit drilling in wilderness areas, so most samples were opportunistically taken from small steps and ledges in outcrops, and we were rarely able to sample key relationships such as crosscutting dikes.

Microstructures of several aplite samples were imaged optically and with backscattered electrons (BSE) and cathodoluminescence (CL) using a Tescan VEGA 5136 scanning electron microscope at UNC. Secondary electron images were acquired with a Zeiss Supra 25 field-emission scanning electron microscope at UNC. Electron microprobe data and BSE and CL images were collected on a JEOL JXA-8530F Hyperprobe at Fayetteville State University with an accelerating voltage of 15 kV. Typical beam size was 1 μm. Whole-rock analyses were performed by Actlabs (Ontario, Canada) by ICP-MS.

Photographs of field exposures were analyzed using ImageJ (https://imagej.nih.gov/ij). Photographs were converted to 16-bit grayscale images and contrast-enhanced, then processed using a 3 × 3 Sobel edge-detection filter.

Results

Dike field relations and relative timing

High-silica dikes of aplite, leucogranite, and pegmatite are common throughout the TIS (Fig. 1). Although their overall areal abundance is only a few percent, they locally make up 50% or more of hectare-sized areas (e.g., Fournier 1968; Coleman et al. 2005; Bartley et al. 2018). Dikes range in thickness from centimeter- to meter-scale. Dips were rarely determinable in the study area owing to two-dimensional exposure, but most felsic dikes in nearby areas of excellent three-dimensional exposure (Half Dome, Glazner et al. 2018; Moraine Dome, Bartley unpublished data) dip moderately (30°–60°) toward the NW or SW. Many have pegmatitic sections with individual crystals several cm or more across, although pegmatite is greatly subordinate to aplite. Many dikes that are nominally designated "aplite" in the field (e.g., Kistler 1973) are really leucogranite (alaskite of Fournier 1968), with median quartz and feldspar grain sizes of several mm or more, and crystals that span the thickness of the dike. The distinction between aplite and leucogranite dikes is completely gradational, with fine-grained sugary aplites grading into coarse-grained leucogranites through locally porphyritic intermediate stages. Pegmatite dikes are considerably coarser than the other two types and are distinguished by blocky alkali feldspar crystals surrounded by anhedral quartz.

The fine-grained dikes have sharp planar contacts and are obviously intrusive, whereas the contacts of leucogranite dikes (i.e., those with grain sizes comparable to the granodiorite host) are rough at the grain scale. We interpret the latter also to be dikes because they share all other field characteristics of the aplites, i.e., tabular shape, truncation of wall rock markers, jogs, T-intersections, and so forth, and because they have the same distinctive trace element characteristics that distinguish aplites from rhyolites, as we show in a later section.

All of the dikes are spatially associated with steeply plunging, epidote- and chlorite-altered pipe structures

(Mustart and Horrigan 2000; Glazner et al. 2011). These range from tens of cm to a few m in diameter, plunge steeply, and typically occur in the centers or along the margins of dikes (Fig. 1).

Intersecting dikes are common, and in some exposures three or more sets can be discerned (Fig. 2). Image processing of outcrop photographs is an effective way to recognize multiple dike generations. In edge-detection images (Fig. 2B, D, F), younger dike generations are darker and more uniform (fewer edges owing to fewer dark mineral grains). Such images reveal subtle dikes that are difficult to recognize in the field.

In areas with intersecting aplite and leucogranite dikes, younger dikes are almost without exception finer-grained or similar in grain size to older ones (Figs. 2, 3), whereas age relations of pegmatite dikes do not fit this pattern.

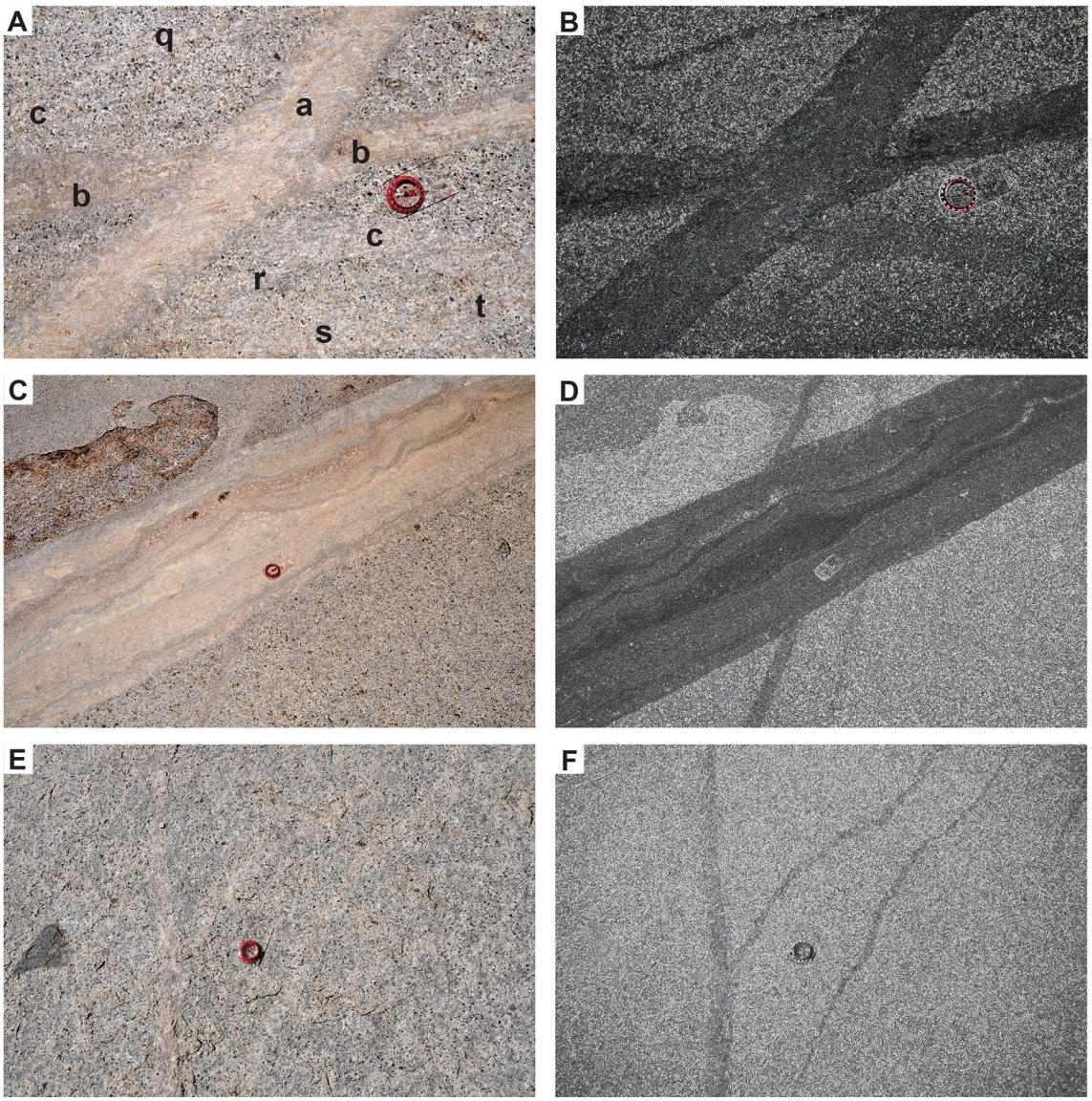

Fig. 2 Photos of multiple dike sets. Note low abundance of dark gray/black minerals in dikes, which makes them dark when edge-detection filtered. Faint glacial striations cross images A and B at an azimuth of ~ 250°. **A**, **C**, **E** Original images with contrast enhanced. **B**, **D**, **F** Find Edges filter applied in ImageJ (3 × 3 Sobel edge detection algorithm). In pair **A**, **B**, note how aplite (a) dike is sharply delineated, whereas leucogranite dikes (others) are not. For dikes a–c, dike c, which is as coarse-grained as the host granodiorite and has irregular, feathered margins, was first, followed by dike b (also coarse, but more distinct), and then sharply defined, fine-grained aplite dike a. The order of intrusion of dikes q–t is unclear; all are coarse-grained, with diffuse margins and grain sizes matching the host granodiorite. **C**, **D** A composite aplite dike ~ 50 cm thick cuts a fainter, coarser-grained 4-cm dike; to its right is a very faint dike with grain size equivalent to that in the host granodiorite. **E**, **F** Faint, branching, coarse-grained leucogranite dikes, 2–5 cm thick. Such dikes are abundant in this area but easily missed during field work. Compass circle is 5 cm in diameter

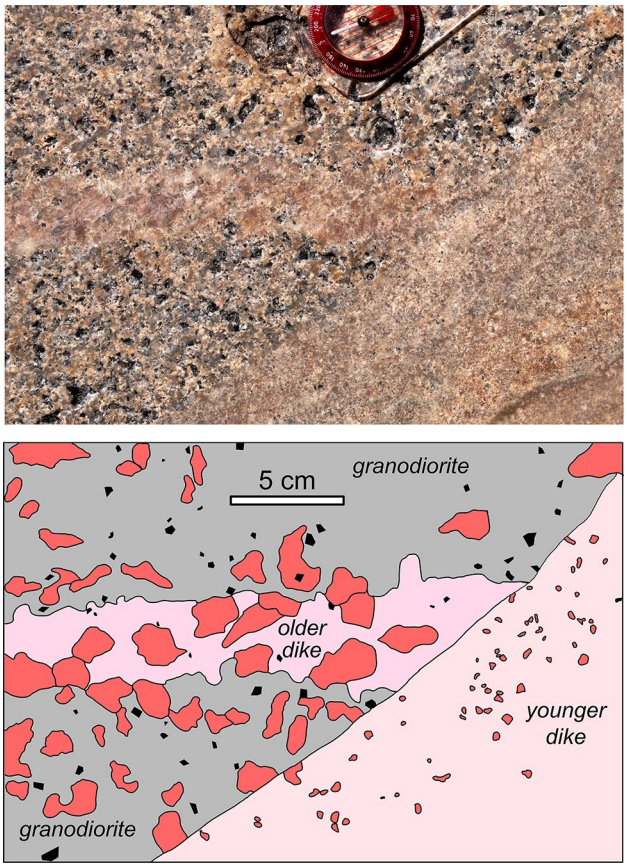

Fig. 3 Closeup of dike intersection (top) and corresponding map (bottom). Feldspar blobs (red) demarcate areas of continuous K-feldspar recognizable on the photograph; not all were mapped. K-feldspar width in the older dike and host granodiorite is roughly a factor of 10 larger than in the younger aplite dike. Note irregular margin of older dike, which contrasts with the sharp, planar margin of the younger one. Large K-feldspar crystals cross the contact between the older dike and host, whereas they are cut-off at the margin of the younger dike. We interpret the coarse grain size and crenulated margin of the older dike to be a result of extensive recrystallization and crystal coarsening of an originally fine-grained aplite dike

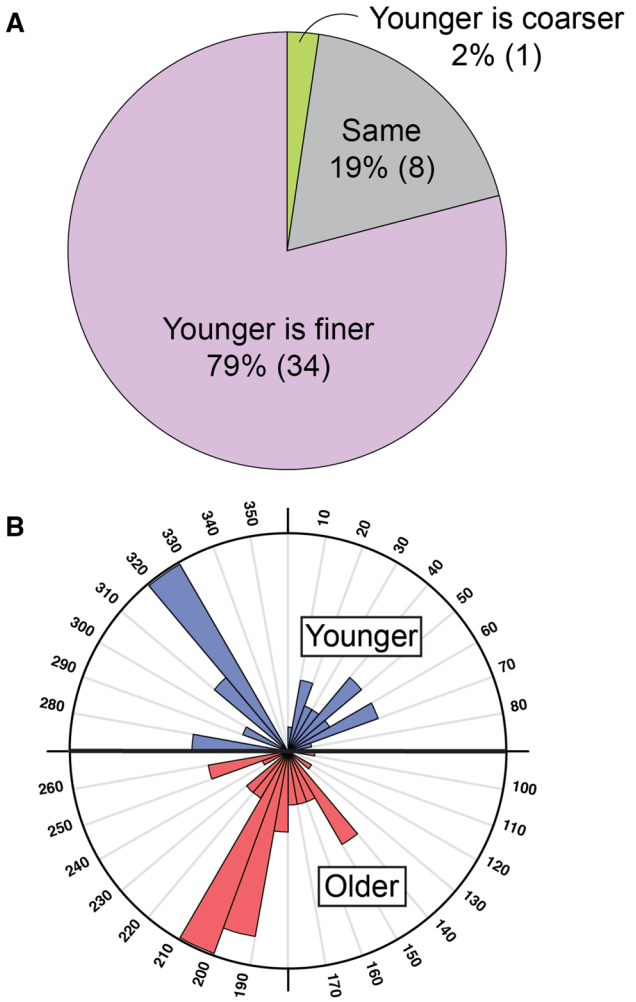

Fig. 4 **A** Summary of grain size relations of intersecting dikes. In all but one case where there was a distinct grain size difference, the younger dike is finer-grained. **B** Rose diagrams of dike trends. The systematic orientation shift from southwest in older dikes to northwest in younger dikes suggests a shift in the principal stress axes with time

We examined 78 dike intersections where relative age and grain size could be determined by inspection in the field, 55 of which did not involve pegmatites (Fig. 4a). Of these, the younger dike is noticeably finer-grained in 80%. In only one was the older dike noticeably finer-grained; in the remaining 20% of cases the grain size distinction was ambiguous. The coarser grain size of the older dikes is invariably accompanied by less well-defined margins (Fig. 3). Younger, aplitic dikes are easily recognized by their fine grain size, sharply defined margins, and low proportions of mafic minerals, whereas older dikes, with grain sizes comparable to the host granodiorite, are ghostly and are most easily recognized by their relative lack of mafic minerals, especially in edge-detection images (Figs. 2, 3).

Dike azimuths were measured at each location; true strike and dip were difficult to determine in most cases owing to low relief on polished surfaces. The youngest dikes at the various stations define a strong maximum at ~ 325°, whereas the maximum for the second youngest dikes is oriented ~ 200° (Fig. 4b). Pegmatite dike azimuths are highly scattered. Given these differences, hereafter we consider only dikes in the aplite–leucogranite spectrum.

Microstructures

Microstructures that are typical of all felsic dikes that we have sampled are illustrated by transmitted light, BSE, and CL images of aplite samples in Figs. 5 and 6. Feldspar grains tend to be roughly equidimensional with smoothly curved

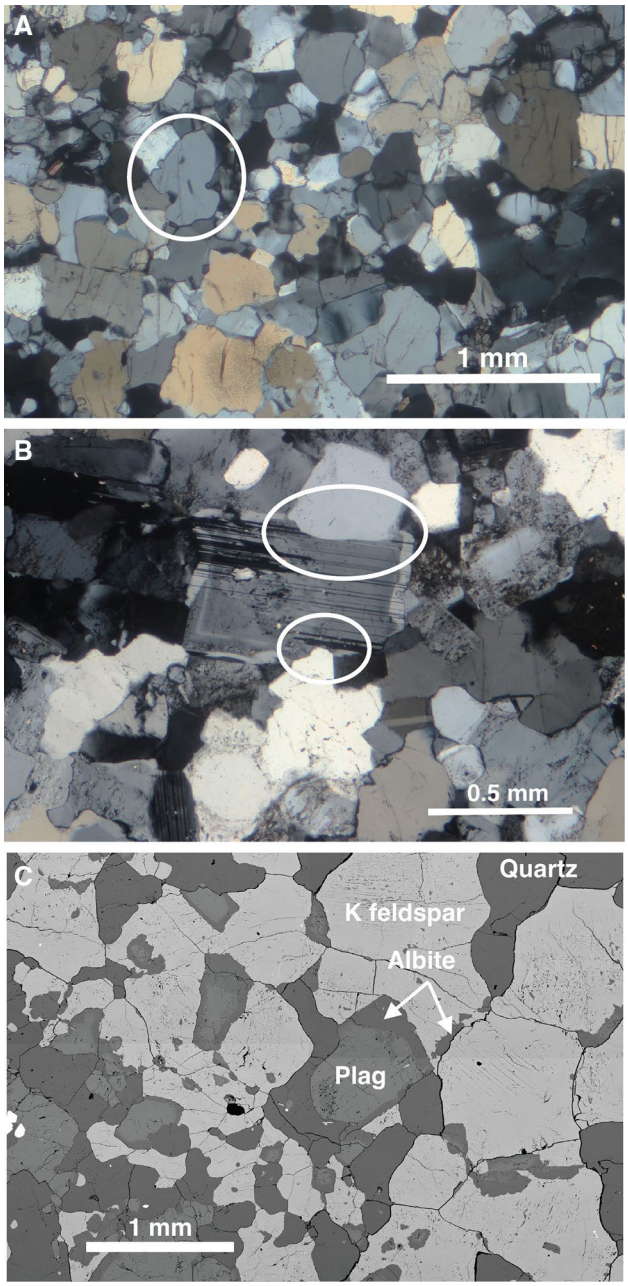

Fig. 5 Microstructures of aplites dikes in the study area. **A** Optical photomicrograph, sample TL11-19, crossed polars. Note the sinuous boundaries of circled quartz grain, and more generally the near absence of straight grain boundaries between any of the major minerals. **B** Optical photomicrograph, sample Y06-39, crossed polars. Note truncation of light-colored rim in the plagioclase by impinging quartz grains (circled). We suggest that impingement was accommodated by dissolution of the plagioclase. **C** Backscattered electron image, sample KR04-13. Albite forms ubiquitous selvages between plagioclase and K-feldspar and also sporadic ragged masses along boundaries between adjacent K-feldspar grains

to irregular grain boundaries; straight grain boundaries are rare. Quartz grains tend to be more irregularly shaped than feldspars, but crystals of all three phases locally have sharp corners or cusps where they meet the boundary of two adjacent grains, i.e., low dihedral angles between the adjacent grains are common (cf. Holness and Vernon 2015).

The complex history of even fine-grained aplite dikes is evident in BSE–CL pairs (Fig. 6). Plagioclase crystals display only weak zoning under cross-polarized light, but CL commonly reveals truncated zoning in plagioclase, K-feldspar, albite, and quartz. Quartz grains are transected by low-CL bands that bound blocks of slightly higher CL material, a texture that Valley and Graham (1996) interpreted to record internal brecciation and healing. Quartz with this texture commonly is enclosed by a CL-dark rim that locally thickens to fill corners between adjacent feldspar grains. Plagioclase and K-feldspar are almost invariably separated from each other by a selvage of nearly pure albite. Contacts between albite selvages and the adjacent feldspars are knife sharp at the μm scale (Fig. 7). Ragged masses of albite also locally occur along boundaries between adjacent K-feldspar grains and within their interiors; such masses are rare in plagioclase.

Both plagioclase and K-feldspar occur in smooth and hole-ridden ("Swiss cheese") forms. CL images of the smooth varieties are simple whereas hole-ridden forms are highly complex, with textures that suggest brecciation and fluid infiltration. Examination of broken surfaces with secondary electron imaging (Fig. 8) reveals that feldspars are riddled with μm-scale voids that are at least locally cleavage-controlled.

Whole-rock and mineral compositions

We were able to collect five medium- to coarse-grained leucogranite dikes, in addition to numerous other previously analyzed aplite dikes from the study area (Glazner et al. 2008), to test whether the leucogranite dikes have the same distinctive trace element signature borne by aplite dikes throughout the Tuolumne Intrusive Suite (we emphasize that finding collectible dike samples from these glacially polished slabs is difficult). Dikes in the Tenaya Lake area have major element compositions that are consistent with aplite and leucogranite compositions worldwide (Tables 1, 2). However, such dikes have distinctive trace element compositions that characterize Sierran aplite dikes derived from titanite-bearing hosts (Figs. 9, 10; Glazner et al. 2008). In particular, they have low Y and middle rare earth element (REE) concentrations and relatively high Sr compared to leucogranite plutons (Coleman et al. 2012).

K-feldspar crystals in the dikes have highly potassic compositions (Table 1; Fig. 11) that are comparable to those in K-feldspar megacrysts (Glazner and Johnson 2013). As with megacrysts, K-feldspar in the dikes is quite low in Ca, with ~ 0.1% An component. Plagioclase is oligoclase or albite.

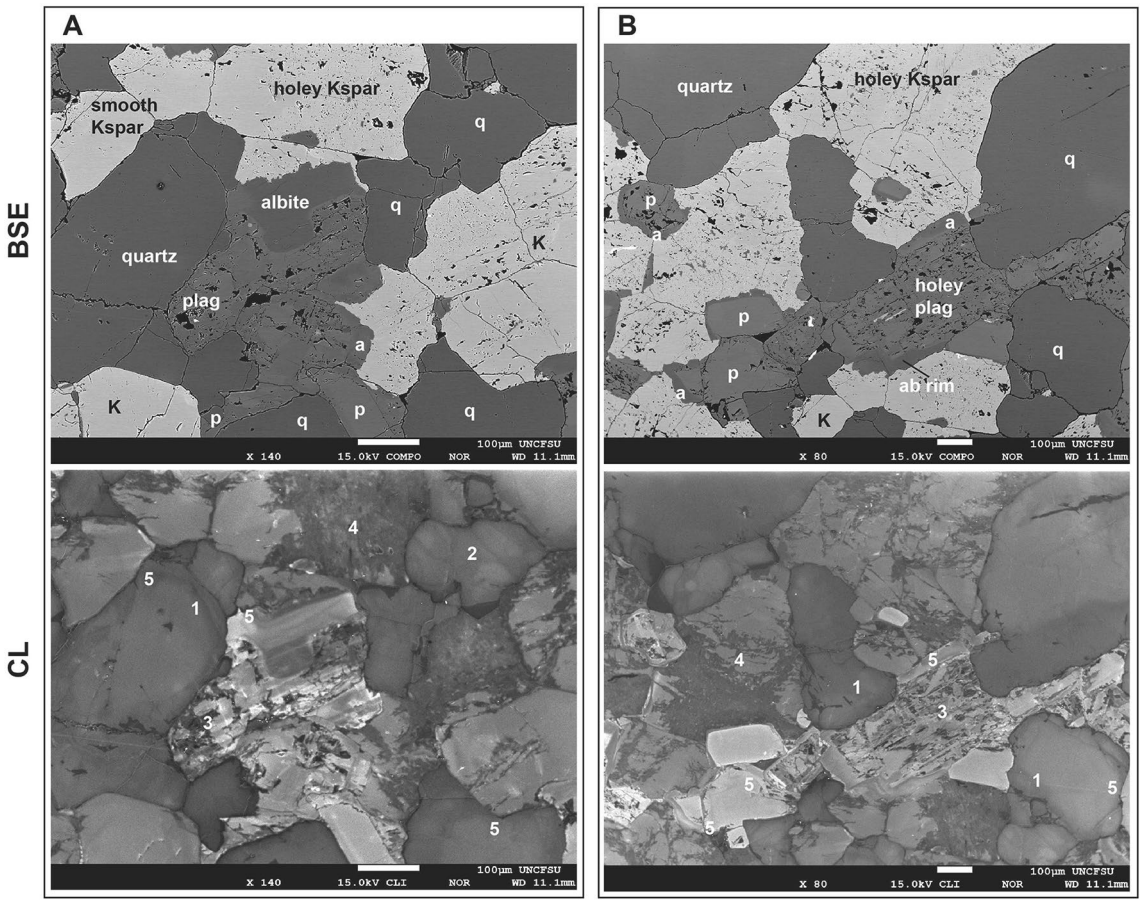

Fig. 6 BSE and CL image pairs showing complex microstructure in aplite dikes. Image pairs A and B from sample Y06-39. Numbers refer to specific features in the figure. Plagioclase and K-feldspar both occur in smooth and holey "Swiss cheese" forms in BSE images, whereas albite and quartz are mostly free of cavities. Quartz shows subtle, complex zoning (1) and apparent brecciation (2) in CL. Holey forms of plagioclase and K-feldspar show extreme internal complexity in CL (3, 4). Truncated zoning (5) is common in CL images of quartz, albite, and locally plagioclase

Discussion

Aplite infiltration

Several mechanisms have been proposed to account for petrological variability in zoned plutonic complexes (e.g., Bateman and Chappell 1979; Stephens and Halliday 1980; Zorpi et al. 1989; Sisson et al. 1996; Gray et al. 2008; Clemens and Stevens 2012); all involve some combination of crystal–liquid separation, contamination, magma mixing, and partial melting. Here, we propose an additional process: *aplite infiltration*, in which late-stage aplite melts are redistributed in a highly crystalline and fractured matrix, after which their presence may be obscured by recrystallization (Fig. 12). Michael (1984) noted that aplite dikes in the Cordillera del Paine complex of Chile are consistent with their being liquids separated from their host granite, but did not have sufficient field access to those remarkable cliff exposures to observe the recrystallization that we document here.

The main points of this paper are that aplite infiltration is pervasive, is responsible for much of the bulk-rock compositional variability of the Half Dome Granodiorite, and occurred at the level of emplacement. Specifically

1. a large volume of the Half Dome Granodiorite—perhaps 25% or more, based on mapping by Coleman et al. (2012)—is leucogranite that formed either by pervasive aplite infiltration or via intrusion of myriad cm- to m-scale aplite dikes;
2. many of these dikes are recrystallized to leucogranite with typical grain sizes on the order of several mm or more;
3. progressively older generations of recrystallized dikes are increasingly difficult to detect owing to grain sizes comparable to, and margins interdigitated with, the host granodiorite; and
4. textures and mineral compositions of even the latest finest-grained aplite dikes indicate extensive recrystal-

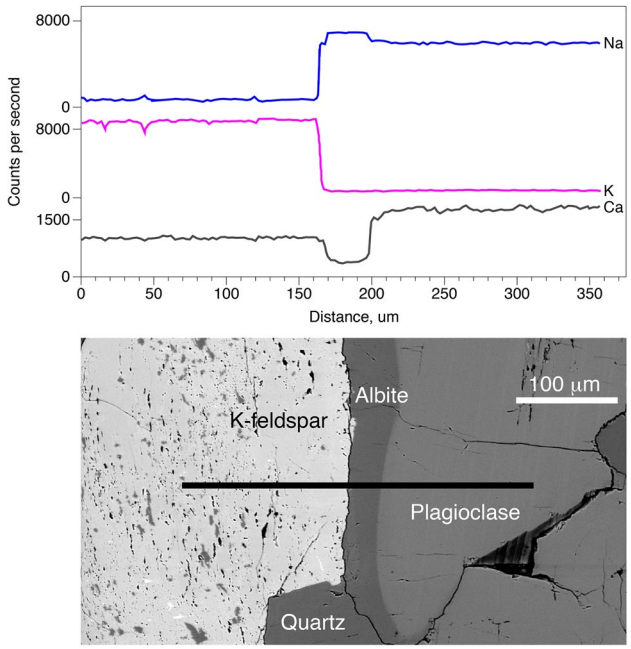

Fig. 7 Analytical traverse across plagioclase–albite grain boundary showing sharp (non-diffusional) contact

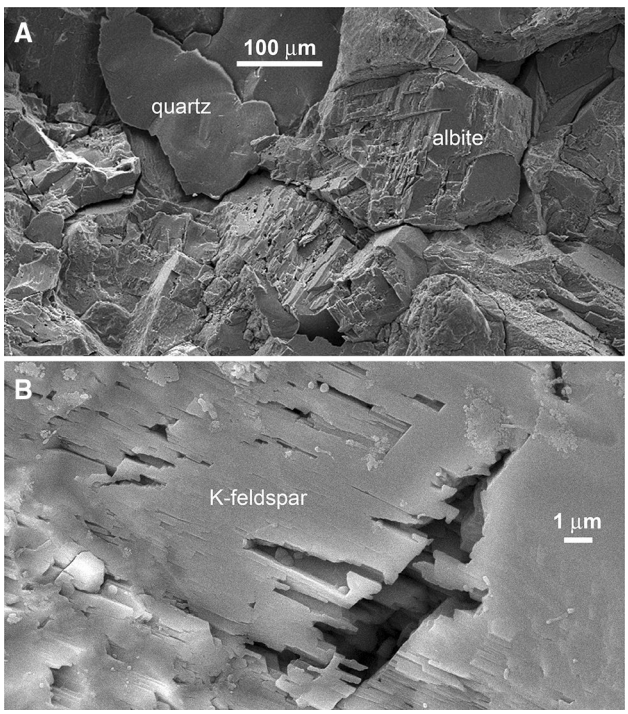

Fig. 8 Secondary electron images of albite and K-feldspar crystals showing abundant cavities and microporosity. Such porosity is important to mineral replacement reactions (Ruiz-Agudo et al. 2014) and is ubiquitous in feldspars in the studied aplite and leucogranite dikes

lization and equilibration of feldspars at temperatures on the order of 400 °C.

Source and significance of the silicic dikes

All felsic dikes analyzed in this study, regardless of grain size or texture, share the same distinctive low-Y, low-middle-REE trace element geochemistry (Figs. 9, 10; Table 2). Glazner et al. (2008) showed that aplites throughout the Sierra Nevada, including several from the study area, have trace element compositions that are distinct from rhyolites, although their major element compositions are comparable. In particular, aplites have low Y abundances and deep scoop-shaped REE patterns with only minor or negligible Eu anomalies, consistent with separation from titanite-bearing crystal assemblages. The presence of these trace element characteristics in thin, coarse-grained leucogranite dikes indicates that the aplites and coarser-grained dikes reflect extraction from a similar solid matrix. Thin leucogranite dikes with grain sizes approaching 1 cm differ from aplite dikes only in grain size, not in composition (Fig. 9).

The high-silica end of the compositional cycles studied by Coleman et al. (2012) is leucogranitic in composition, with > 75 wt% SiO_2 and ~ 4 wt% K_2O, but has the low Y and low middle REE that characterize aplites. Thus, although the high-silica end of a Half Dome cycle was produced by crystal–liquid separation, it is not equivalent to erupted rhyolite and a global survey shows that liquids of this composition do not erupt (Glazner et al. 2015). Within a compositional cycle, there is a pronounced upward increase in the volumetric proportion of silicic dikes relative to the intruded granodiorite, and as noted earlier, the dikes form a complex network in which crosscutting relations indicate myriad episodes of injection during differentiation to form a cycle. Dikes become difficult to distinguish in the field in the uppermost leucogranitic parts of the cycles because they largely intrude older dikes of similar composition. Therefore, dike relations reported in this study and by Bartley et al. (2018) are located in the transition from mafic to felsic parts of a cycle where there is clearer contrast between dikes and their wall rocks.

Importance of recrystallization by dissolution–reprecipitation

In field and microscope examination, the dikes have typical igneous textures (Figs. 1, 2, 5, 6). However, data summarized below indicate that these textures have been significantly recrystallized.

A growing body of evidence demonstrates that dissolution–reprecipitation (hereafter DR) is an important, and perhaps dominant, mechanism by which less-stable minerals are replaced by more stable ones (e.g., Putnis 2002;

Table 1 Electron microprobe analyses of K-feldspar and plagioclase in medium- to coarse-grained leucogranite dikes

Sample	KR04-13		KR04-16		TL11-19		Y06-39		Y06-40	
Latitude	37.8274		37.8540		37.8319		37.8341		37.8311	
Longitude	− 119.4745		− 119.4543		− 119.4705		− 119.4685		− 119.4662	
	K-fsp	Plag	K-fsp	Plag	K-fsp	Plag	K-fsp	Plag	K-fsp	Plag
SiO_2	66.31	66.95	66.75	67.00	66.28	65.08	65.61	68.43	66.77	66.88
Al_2O_3	18.10	21.63	18.26	21.88	17.99	22.22	17.93	20.31	18.22	22.06
FeO^t	0.06	0.08	0.07	0.12	0.06	0.10	0.06	0.05	0.05	0.09
CaO	0.01	2.63	0.01	2.79	0.02	3.62	0.00	1.39	0.03	3.21
Na_2O	1.04	9.58	0.98	9.23	1.07	8.83	0.93	10.55	1.09	9.51
K_2O	14.25	0.45	14.36	0.39	14.27	0.35	14.03	0.21	13.97	0.38
BaO	0.00	0.01	0.02	0.02	0.05	0.01	0.05	0.01	0.12	0.00
An	0.03	12.82	0.07	13.99	0.08	18.10	0.03	6.71	0.14	15.40
Ab	10.00	84.56	9.39	83.65	10.19	79.83	9.12	92.11	10.55	82.46
Or	89.97	2.62	90.54	2.36	89.73	2.07	90.85	1.18	89.31	2.14

Oxides in wt%; feldspar components in mol%

Ruiz-Agudo et al. 2014). For example, even in a relatively fast-diffusing system such as alkalis in K-feldspar and albite, complete replacement of one by the other can occur at low temperatures far faster than solid-state diffusion kinetics allow. O'Neil and Taylor (1967) suggested that alkali exchange among alkali feldspars occurs via dissolution of the less-stable phase at the fluid–crystal interface followed by precipitation of the more stable phase (i.e., DR) rather than by solid-state diffusion. Observations and experiments demonstrate that this mechanism is widespread and likely the dominant way in which mineral replacement occurs in a wide variety of systems (Ruiz-Agudo et al. 2014). In low-temperature systems analogous to magmas, DR can be observed in real time, especially if temperature is cycled (Donhowe and Hartel 1996; Mills et al. 2011).

The compositions of K-feldspar crystals in granites sensu lato indicate that DR is widespread and pervasive. In K-feldspar megacrysts, the anorthite component (An) is much lower, and the orthoclase component (Or) much higher, than in volcanic rocks of comparable composition (Glazner and Johnson 2013). Glazner and Johnson showed that solid-state diffusion of An out of the crystals is orders of magnitude too slow to account for their low An contents, and proposed DR as an alternative method for reforging the crystals. In the Tenaya Lake area, K-feldspar in aplite and leucogranite dikes and in the host granodiorite is similarly An-poor and Or-rich, and we suggest that DR is a pervasive process in remaking the compositions of K-feldspar crystals in the aplite and leucogranite dikes and in the host granodiorite.

Cause of recrystallization

As noted above, observations in the Tenaya Lake area show that some K-feldspar megacrysts were broken by silicic dikes and then healed across the fracture (Glazner and Johnson 2013, their Fig. 13), and this process is widespread in granites (Hibbard and Watters 1985; Pitcher 1993). Abundant mineralogical and phase-equilibrium evidence that K-feldspar megacrysts in the Tuolumne Intrusive Suite chemically equilibrated at temperatures on the order of 400 °C or lower (Glazner and Johnson 2013), and Ackerson et al. (2018) provided evidence that quartz in TIS granodiorites crystallized down to temperatures < 500 °C. These observations provide further evidence of extensive crystallization and recrystallization at temperatures near and below the nominal granodiorite solidus.

Recrystallization of both the dikes and the host granodiorite was probably driven by protracted residence at elevated and fluctuating temperatures and by elevated water fugacity. Thermochronology indicates that many large Sierran plutons remained above biotite Ar closure (~ 300 °C) for 8–10 Ma (Davis et al. 2012), consistent with thermal modeling of incremental growth (e.g., Annen 2011). This provides ample time for textural modification by static recrystallization. Furthermore, episodic addition of magma to the pluton causes temperature and water fugacity fluctuations that would promote episodic DR near the site of emplacement. Fluctuations of temperature are an effective means of grain coarsening (Donhowe and Hartel 1996; Mills and Glazner 2013; Erdmann and Koepke 2016), and thus likely contributed to growth of K-feldspar megacrysts and coarsening of early silicic dikes. Ubiquitous hydrothermal pipes in the TIS (Mustart and Horrigan 2000; Glazner et al. 2011) are evidence of both transport mechanisms: their immediate cause is rock alteration by infiltration of an aqueous fluid, but their close and persistent spatial association with silicic dikes indicates that the dikes and water followed similar pathways.

Table 2 Chemical analyses of leucogranite dikes

Sample	TL11-2A	TL11-2B	TL11-6B	TL11-19	TL11-20
SiO_2	75.17	75.27	75.04	74.13	76.01
TiO_2	0.15	0.17	0.11	0.06	0.05
Al_2O_3	13.13	13.69	14.33	14.61	13.01
$Fe_2O_3^t$	1.49	1.27	0.99	0.57	0.66
MnO	0.03	0.02	0.02	0.01	0.01
MgO	0.34	0.32	0.17	0.10	0.05
CaO	1.48	1.64	1.97	1.53	0.83
Na_2O	3.06	3.25	3.68	3.29	3.03
K_2O	4.74	4.58	3.95	5.48	5.66
P_2O_5	0.04	0.03	0.04	0.01	0.00
LOI	0.58	0.60	0.50	0.40	0.23
Total	100.20	100.80	100.80	100.20	99.54
V	29	19	17	9	12
Ga	16	15	15	14	16
Rb	156	155	118	163	189
Sr	230	280	303	326	75
Y	2.7	2.8	2.5	1.2	1.2
Zr	83	70	52	28	57
Nb	2.6	3.6	1.9	1	1.7
Cs	4.5	7.6	3.5	7.7	5.5
Ba	314	356	326	561	82
La	18	33	9.38	9.36	7.9
Ce	22.2	29.1	13.8	10.7	8.28
Pr	1.71	2	1.34	0.84	0.56
Nd	4.96	5.72	4.58	2.49	1.54
Sm	0.78	0.93	0.79	0.36	0.29
Eu	0.237	0.248	0.213	0.163	0.07
Gd	0.5	0.71	0.5	0.23	0.14
Tb	0.08	0.09	0.07	0.04	0.02
Dy	0.46	0.5	0.4	0.23	0.13
Ho	0.08	0.09	0.07	0.04	0.03
Er	0.24	0.27	0.2	0.11	0.11
Tm	0.045	0.043	0.031	0.019	0.019
Yb	0.31	0.35	0.26	0.13	0.16
Lu	0.054	0.072	0.047	0.021	0.036
Hf	3.9	2.6	1.8	1.1	2.8
Ta	0.27	0.38	0.2	0.11	0.16
Pb	27	31	28	32	40
Th	23.3	29.4	20	18.3	29.8
U	9.35	6.81	10.1	7.57	13.6

All samples from a hectare-sized area centered on 37.8056, -119.4697. Major-element oxides, V, Sr, Ba by fusion ICP; all others by fusion ICP-MS. Oxides in wt%, elements in parts per million by weight

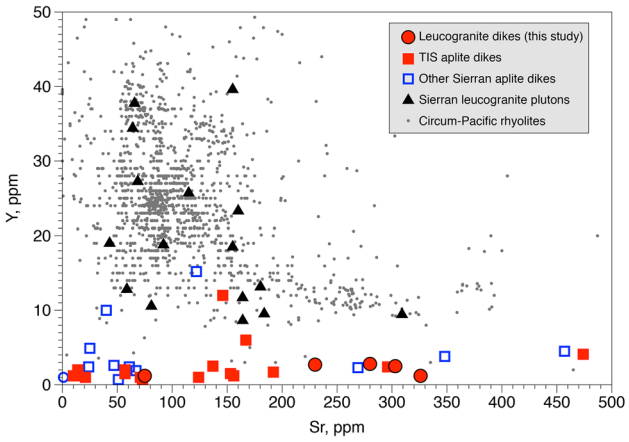

Fig. 9 Plot of Y vs. Sr for leucogranite dikes from this study, Sierran aplites from Glazner et al. (2008), Sierran leucogranite plutons (Coleman et al. 2012) and Circum-Pacific volcanic rocks with SiO_2 between 74 and 78 wt%. Dikes in this study have uniformly low Y, consistent with aplites and unlike leucogranite plutons and erupted rhyolites. Stripes at integer values of Y in the Circum-Pacific set reflect low-precision analyses

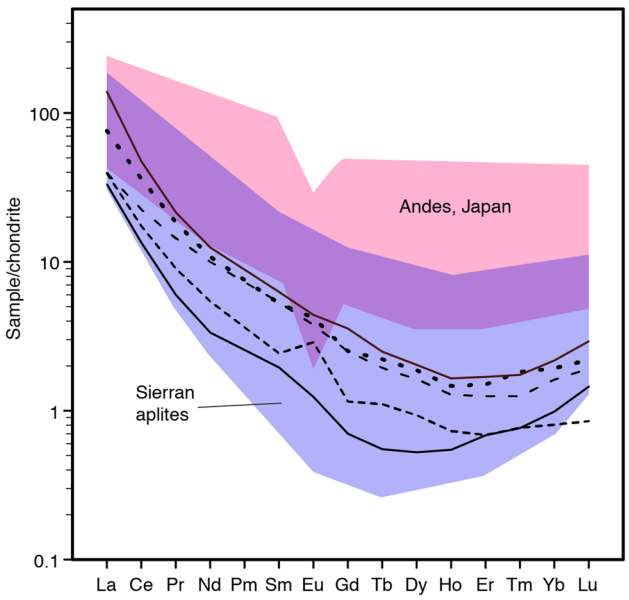

Fig. 10 REE plot of leucogranite dikes from this study compared to fields for (1) rhyolites from the Andean and Japan arcs and (2) Sierran aplite dikes. Leucogranite dikes have low middle and heavy REE, similar to aplites and unlike erupted rhyolites

Evidence for widespread recrystallization throughout this region, and indeed in other plutonic terranes around the world (Pitcher 1993), directly contradicts the contention by Holness et al. (2018) that granitic microtextures represent an essentially unmodified record of down-temperature crystallization. We have provided observational and geochemical evidence that leucogranite veins with typical crystal diameters on the order of 1 cm form by recrystallization of aplite veins with typical crystal diameters of 1 mm or less. Microstructures of aplite veins indicate that they also have been recrystallized, implying that primary igneous textures are at most sparsely preserved anywhere in the pluton.

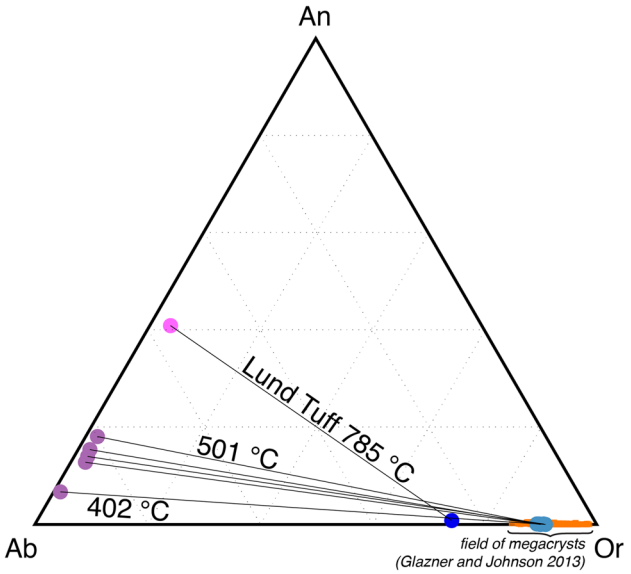

Fig. 11 **a** Compositions of K-feldspar and plagioclase crystals in aplite and leucogranite dikes. Highly potassic K-feldspar indicates low temperatures of equilibration. Plagioclase–K-feldspar pair from the Oligocene Lund Tuff of Nevada and Utah (Maughan et al. 2002), a dacite comparable in composition to the Half Dome Granodiorite, shown for comparison. Dike tie lines are rotated significantly counterclockwise in response to lower temperature. We interpret these temperatures as the lower limit of recrystallization of the feldspars

Evidence from phase equilibria, geochemistry, and field and petrographic observation clearly indicate that K-feldspar megacrysts form late in a magma's supersolidus history (Glazner and Johnson 2013), not early and in an abundance of magmatic liquid, and continue to recrystallize down to temperatures near 400 °C.

Thermobarometry

Zircon separation thermobarometry of aplite dikes in this study, using the technique of Putnam et al. (2015), yields temperatures of 590–670 °C and pressures on the order of 100 MPa. This thermobarometer estimates the temperature at which aplitic melt was separated from zircon-bearing residuum using zircon saturation, and pressure from aplite bulk composition. In contrast, feldspar compositions (Table 1) yield two-feldspar temperatures of 400–500 °C using the Eq. 27b geothermometer of Putirka and Tepley (2008) at an assumed pressure of 200 MPa. We interpret these temperatures to record the lower limit of recrystallization of the feldspars, well down the ternary solvus (Glazner and Johnson 2013).

Ackerson et al. (2018) calculated crystallization temperatures of 475–560 °C for quartz in the Cathedral Peak Granodiorite of the TIS, and London et al. (2020) calculated temperatures of 375–475 °C for feldspar pairs in pegmatite dikes and concluded that they represent crystallization temperatures of the pegmatite-forming melts. Thus, a growing body of data indicates that late-stage quartz-feldspar assemblages in granitic rocks continue to equilibrate down to temperatures 100–250 °C below the nominal water-saturated granite solidus.

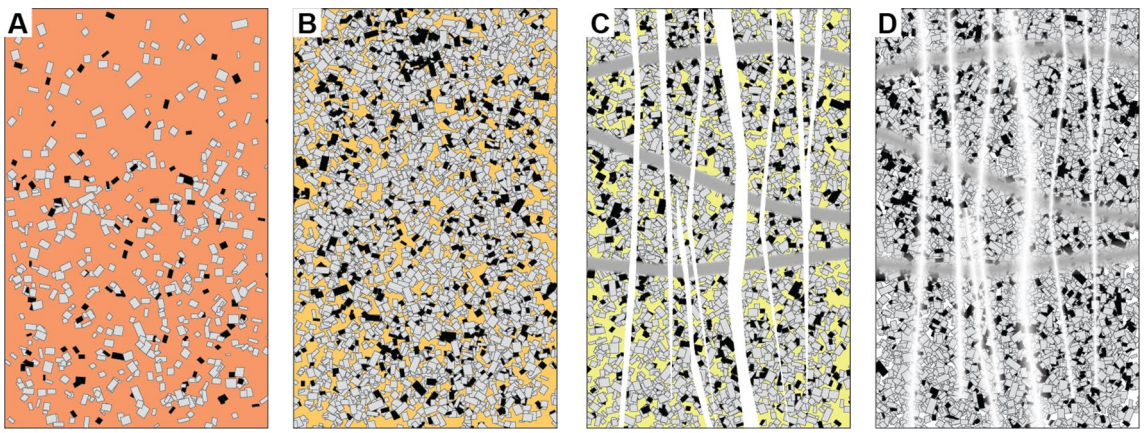

Fig. 12 Schematic cross-sections illustrating late-stage aplite infiltration in the study area. **a** Crystallization produces a significant crystal fraction and silica-rich interstitial liquid. Buoyant rise of liquid via compaction and porous flow produces the large-scale (hectometer to kilometer) bulk-rock compositional variation documented by Coleman et al. (2012). **b** As crystal fraction grows beyond 50%, a static crystal framework (rigid sponge) with high-silica interstitial liquid forms. Compaction is greatly inhibited owing to the rigid crystal framework, and porous flow by increasing tortuosity of flow paths. Further differentiation is slow. **c** Buildup of volatile pressure in the interstitial liquid eventually overpressurizes the system (Eichelberger et al. 2006), cracking the crystal matrix (Hibbard and Watters 1985) and allowing injection of high-silica aplite liquid into cracks that rapidly transport it upward, resulting in a late pulse of efficient crystal–liquid segregation. **d** Solidified product, in which dike margins have interdigitated with the surrounding rock and older dikes have attained grain sizes comparable to the host rock, as in Figs. 2 and 3

Significance and source of albite selvages

Rims of nearly pure albite on other feldspars are ubiquitous in granitic rocks (Rogers 1961; Peng 1970; and references therein). In dikes of the Tenaya Lake area, and indeed in all granitic rocks of the TIS, these selvages are visible in cross-polarized light and in BSE and CL imaging (Figs. 5c, 6, 7). When such images are false-colored to highlight the spatial distribution of albite (Fig. 13), it is clear that the selvages only occur at contacts between K-feldspar and plagioclase, and are present along > 95% of such contacts. They are not seen at contacts between quartz and either plagioclase or K-feldspar.

Albite rims have been explained as forming either via exsolution from other feldspars or as the last stage of crystallization of magmatic liquid (Peng 1970). Rogers (1961) pointed out that the former explanation does not account for their presence only along plagioclase–K-feldspar boundaries. However, the latter does not explain why pure albite would form at all, because sodic feldspar in equilibrium with K-feldspar is generally no more sodic than $An_{15–20}$ (Carmichael 1963).

X-ray scans across K-feldspar–albite–plagioclase boundaries show that compositional variations across grain boundaries are sharp at the scale of a few μm (Fig. 7). Sharp grain boundaries commonly result from DR. For example, Niedermeier et al. (2009) and Hövelmann et al. (2010) studied cation exchange among alkali feldspars and replacement of plagioclase by albite under hydrothermal conditions and found sharp interfaces between phases.

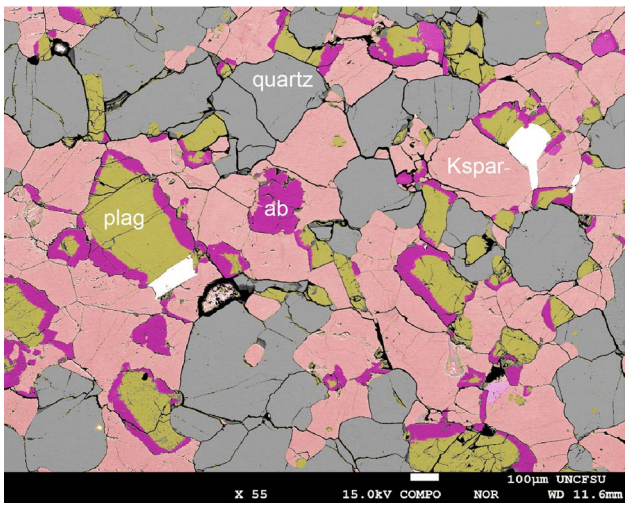

Fig. 13 False-color BSE image of sample TL11-19 highlighting albite (ab; magenta), which is ubiquitous along contacts between plagioclase (plag; yellow) and K-feldspar (Kspar; pink) and not found along contacts between quartz and either plagioclase or K-feldspar. Patches of albite also occur within K-feldspar. White patches are Fe-bearing minerals

Mass balance calculations indicate that the albite selvages could be derived entirely from the original high-temperature K-feldspar. Figure 13 is a representative of the aplite–leucogranite dikes. Albite makes up ~ 7 area% of this image, and K-feldspar 38 area%. If the K-feldspar above the solidus had been Or_{70}, removing 22 vol% albite would convert it to Or_{90}. This corresponds to ~ 10 vol% albite, roughly the observed proportion. Consistent with the hypothesis of Glazner (2019), we propose that down-temperature recrystallization precipitates more potassic K-feldspar, and that the albite eliminated from the K-feldspar reprecipitates preferentially at contacts between plagioclase and K-feldspar as a mechanism to minimize the surface energy costs of such contacts.

Significance of microstructures

Holness and Vernon (2015) and Holness et al. (2018) dismissed coarsening of granitic rocks after magmatic crystallization based on the assumption that such textural modification is driven by minimization of surface energy (i.e., Ostwald ripening) which in turn is likely only effective for μm-scale crystals (e.g., Cabane et al. 2005). They argued that grain growth by Ostwald ripening should eliminate low dihedral angles and that, because low dihedral angles are observed in granitic textures, Ostwald ripening cannot be important in granitic rocks.

This analysis is largely irrelevant to late-stage processes in a granitic pluton for two reasons. First, dismissal of Ostwald ripening is generally based on its inefficiency at constant temperature, but evidence from a wide variety of fields in materials science shows that small temperature variations facilitate significant crystal coarsening via DR (e.g., Donhowe and Hartel 1996; Mills and Glazner 2013). Second, surface energy is not the only energy source available to drive late-stage textural modification of granites. Surface energy effects alone may be insufficient to cause significant crystal ripening under late-stage conditions (but see Boudreau 2011), but there is clear evidence that other processes are at work. As pointed out by Glazner and Johnson (2013) and reiterated here, primary igneous minerals in granites invariably have undergone extensive low-temperature modification. Energy released by these late-stage mineral reactions (e.g., exsolution; component exchange driven by changes in temperature) and the chemical potential gradients that they generate in pore fluids undoubtedly plays a central role in modification of primary igneous textures in granites.

Significance of crosscutting relations

Compositionally cyclic magmatic rocks in the Half Dome Granodiorite range in age over 3–4 Ma (Coleman et al. 2004,

2012), and each cycle contains multiple generations of crosscutting silica-rich dikes. This indicates that upward transport of felsic melt to form the compositional cycles took place throughout assembly of the pluton rather than only at a late stage.

Several other lines of evidence reinforce the inference that the dikes formed over timescales on the order of 10^6 years. For example, earlier dikes differ systematically in their orientations from later ones in a pattern that is uniform over an area of at least several square kilometers (Fig. 4b). This change in dike orientation implies a change in ambient stress state throughout a significant volume of rock. Detailed mapping of felsic dikes within one cycle (Bartley et al. 2018) revealed the same dominant trends but with more complex crosscutting relations. The same trends in felsic dike orientation also are present on Half Dome proper (Glazner et al. 2018).

Textural patterns among non-pegmatitic silicic dikes imply emplacement over a time period sufficient to permit thorough recrystallization of originally fine-grained dikes. Crosscutting relations in the Tenaya Lake area show that older generations of dikes are consistently coarser-grained and less distinct than younger ones (Fig. 4a); indeed, where three generations of crosscutting dikes are present, the oldest dikes are commonly distinguishable from the host granodiorite only by a relative lack of mafic minerals because the quartz and feldspar crystals are as coarse as those in the host. Quartz and feldspar crystal dimensions in the thinner leucogranite dikes are comparable to the apertures of the dikes that host them. We interpret these textural relations to indicate recrystallization of older dikes from an originally aplitic texture.

We cannot rule out the possibility that the older, coarser dikes originally crystallized to a coarse grain size, but the consistent crosscutting relations, geochemical fingerprints identical to fine-grained aplite dikes, and ragged margins strongly suggest that the leucogranite dikes are recrystallized aplite dikes. The irregular, indistinct margins of the older dikes, and general correlation between grain size and fading of a sharp margin are difficult to explain otherwise.

Pluton diversity produced by aplite infiltration

The processes that bring about geochemical diversity in igneous rocks have been debated for over a century. These processes include crystal–liquid separation, assimilation, magma mixing, restite unmixing, partial melting with peritectic entrainment, and partial melting with back-mixing (e.g., Bowen 1928; White and Chappell 1977; Chappell 1996; Clarke 2007; Stevens et al. 2007; Gray et al. 2008). Based on the field and geochemical relations described above, we propose infiltration of aplitic liquid (aplite infiltration) as an additional common and important process that modifies the compositions of plutonic rocks.

Aplite infiltration can proceed by two mechanisms, porous flow and diking. If crystal–liquid separation occurs when the proportion of crystals is low enough that there is significant permeability, then the liquid can percolate upward to produce an upward increase in silica, leaving behind a residue that is depleted in silica. We infer that this mechanism contributed to the km-scale compositional cycles in the Half Dome Granodiorite (Coleman et al. 2012).

However, once a magma body crystallizes to the point that there is a solid crystal framework capable of fracture, pore melt ascent must slow dramatically because permeability is greatly reduced and because further compaction requires crystal–plastic deformation. At this point, differentiation will largely cease. However, if the solid matrix is fractured, either by volatile saturation of the magma or by any other mechanism (e.g., tectonic deformation; Bartley et al. 2018), then resulting extraction of aplitic pore melt into the fractures could efficiently rejuvenate differentiation by rapid upward transport of silicic melt in the dying system.

The length scale of aplitic melt transport is difficult to estimate but would have to act over distances of hundreds to perhaps a few thousand meters to explain relationships in the Half Dome Granodiorite. Putnam et al. (2015) found that the trace element characteristics of aplite dikes in intrusive suite of Yosemite Valley reflect that suite's low titanite abundances and not those of the adjoining, younger TIS, indicating that dikes from the TIS did not travel far laterally. It is commonly stated that water-saturated silicic melts cannot rise far because they will freeze upon ascent owing to the negative slope of the water-present solidus (e.g., Cann 1970), but this is incorrect (Tuttle and Bowen 1958; Glazner 2019). Propagation of aplite dikes is probably limited simply by the supply of late-stage melt. Once fractures form and melt moves into them, the sponge has been squeezed and the source has run out.

Eichelberger et al. (2006) proposed that late-stage fracturing and production of aplite dikes occur because vapor exsolution can raise the pore pressure enough to fracture the crystalline matrix. They further noted that rhyolitic melt could be extracted from a given volume of crystallizing magma much more rapidly by channelized flow in dikes than by porous flow and proposed that some rhyolite eruptions occur by extracting melt from dikes rather than from a magma chamber. Although the eruption hypothesis fails because aplites and rhyolites have different trace element compositions (Glazner et al. 2008), channelized dike flow neatly explains the relationships explored here.

This process can produce a high-silica granitic portion and a complementary low-silica melt-depleted residuum from an originally homogeneous mush or rigid sponge (Hildreth 2004). The high-silica portion consists of a network of

high-silica dikes and thus is heterogeneous, but much of the field evidence for this is masked by recrystallization of the initially fine-grained aplite dikes to grain sizes comparable to the host rock. Pervasive diking can lead to rock compositions that are heterogeneous at the centimeter scale but relatively homogeneous at the decimeter and meter scales.

Restriction to plutonic rocks

Aplite infiltration can only occur in crystallizing plutonic rocks—it is not available as a differentiation process for volcanic rocks because it requires a high degree of crystallinity (perhaps > 70%). Thus, we predict that plutonic rocks should show chemical differences consistent with this; in specific, we predict that, among high-silica igneous rocks, only plutonic rocks will show a significant trend toward compositions influenced by infiltration of aplitic melt with low concentrations of trace elements that are retained in the crystalline residuum. In particular, any granitic rock will retain Ba (compatible in K-feldspar) and Zr (in zircon), and titanite-bearing crystalline assemblages will retain most middle REE and Y; thus, high-silica melt derived from these will be depleted in those elements.

To test this hypothesis, we compare plutonic and volcanic rocks from Circum-Pacific convergent margins using the geochemical dataset of Glazner et al. (2015). This dataset was extracted from the Earthchem database (earthchem.org); details of data extraction are given in that paper. On most element–element plots, plutonic and volcanic data are congruent (Glazner et al. 2015; Keller et al. 2015), but key elements differ in detail. Here, we focus on Ba and Zr, two elements that should be retained in the crystalline residuum of most crystallizing granitic magmas when aplitic melt is extracted. Strontium shows a relationship similar to those for Ba and Zr, but is highly scattered.

Figure 14 compares Ba and Zr in plutonic and volcanic rocks from the Circum-Pacific subduction dataset. Volcanic analyses are far more abundant (23,261) than plutonic (1782), so the volcanic points plotted in Fig. 14 have been randomly downsampled to 1782. However, the two-dimensional histogram contours (drawn following the methods of Glazner et al. 2015) use the entire datasets. For both elements, the plutonic pattern takes a steep downturn at high SiO_2, producing inverted hockey stick and boomerang patterns, respectively. Similar patterns are evident when the dataset is reduced to regional scale (e.g., Japan) and to the scale of individual plutons (e.g., Atherton and Sanderson 1987; Bachl et al. 2001; Barnes et al. 2001; Blundy and Ulmer 2006). These high-silica downturns are consistent with separation of liquid from a low-silica crystal mush containing K-feldspar and zircon.

Removal of low-Ba, low-Zr liquid from a crystallizing magma will leave behind a residual magma enriched in those elements. This effect is difficult to see, however, because the proportion of aplitic melt removed is likely 10% or less. As an example, removing 10 wt% aplitic liquid with 200 ppm Ba and 76 wt% SiO_2 from granodiorite magma with 600 ppm Ba and 70 wt% SiO_2 leaves a residuum with 644 ppm Ba and 69.3 wt% SiO_2—scarcely resolvable from the original composition on a plot such as that in Fig. 14.

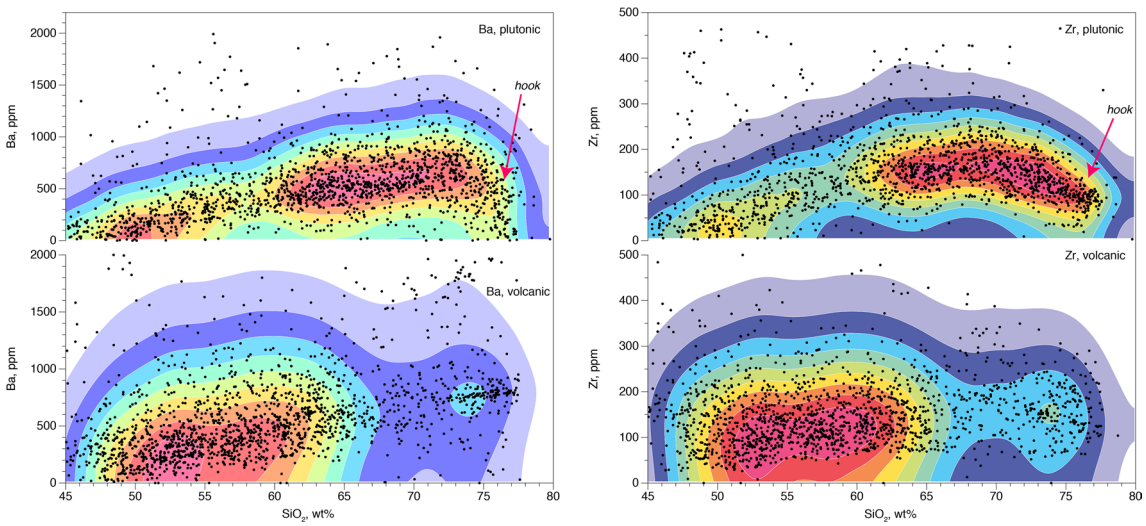

Fig. 14 Comparison of Ba and Zr systematics for plutonic and volcanic rocks from Circum-Pacific subduction zones, using the database of Glazner et al. (2015). The aplite infiltration hypothesis predicts that plutonic rocks will hook downward at high SiO_2 owing to separation of liquid from a residuum bearing K-feldspar and zircon, whereas volcanic rocks will not. These data are consistent with this prediction. Colored contours (2D histograms) were constructed using the method in Glazner et al. (2015), using all data. Because the database has far more volcanic points (23,261) than plutonic (1782), we randomly downsampled the volcanic dataset for plotting individual points

Keller et al. (2015) previously recognized the depletion of these elements at high SiO_2 and attributed it to crystal fractionation. Field and geochemical patterns of the TIS lead us instead to attribute it to a different form of crystal–liquid separation, production of high-SiO_2 rocks by infiltration of aplitic liquids. As with aplites themselves, volcanic rocks of this aplitic trace element composition are essentially absent from the volcanic record (Glazner et al. 2008). Patterns for Y, middle REE, and Sr are similar, but masked by scatter, in part because titanite is not a ubiquitous accessory mineral, and we emphasize that such downward hooks are significantly more common in plutonic rocks than in volcanic rocks. We conclude that trace element geochemical patterns support the infiltration hypothesis as an important method of differentiation that is restricted to intermediate and silicic plutonic rocks.

Conclusions

Silicic dikes in the Half Dome Granodiorite that range in texture from aplite to coarse leucogranite are a significant component of the more felsic portions of the pluton. Field and geochemical evidence indicate that the dikes represent silica-rich pore melt that was expelled from granodioritic crystal mush and ascended buoyantly in dikes. We infer that transport of this silicic melt, both by porous flow and in dikes, was the dominant mechanism of in situ chemical differentiation in the Half Dome pluton.

Multiple generations of geochemically similar, crosscutting silicic dikes are found within each of several compositional cycles in the Half Dome Granodiorite that reflect in situ differentiation during incremental growth of the pluton. This strongly suggests that pore-melt migration operated over the entire duration of pluton assembly. Several characteristics of the dikes reinforce this interpretation, including (a) a systematic shift of dike orientation with time, indicating that dike intrusion spanned a change in the ambient stress regime; (b) progressively finer grain size and more distinct margins in younger dikes, with the oldest dikes texturally indistinguishable from the host granodiorite, suggesting that all of the silicic dikes crystallized with aplitic texture but that older dikes were increasingly recrystallized after their intrusion; and (c) overprinting of some silicic dikes by growth of K-feldspar megacrysts which also are products of post-emplacement recrystallization. The overprinting recrystallization responsible for the coarse grain sizes of early-intruded dikes probably resulted from a long residence time at elevated and fluctuating temperatures within the incrementally growing Half Dome pluton, and from the infiltration of aqueous fluid released by crystallization of younger intrusive increments emplaced inside and below the pluton.

Acknowledgements This work was supported by National Science Foundation Grants EAR-125050 and EAR-0538129 to Glazner and Coleman and EAR- 0538094 to Bartley, and by the Mary Lily Kenan Flagler Bingham Professorship of UNC Chapel Hill. We thank Bryan Law for his excellent observational skills and knowledge of Yosemite National Park, and Dean Eppler for arranging field time, on Earth, for the fourth author. We appreciate constructive reviews by Tom Sisson and Editor Othmar Müntener. As always, National Park Service personnel, especially Greg Stock, Jan van Wagtendonk, and Peggy Moore, have been supportive and helpful to our field studies in Yosemite.

References

Ackerson MR, Mysen BO, Tailby ND, Watson EB (2018) Low-temperature crystallization of granites and the implications for crustal magmatism. Nature 559:94–97. https://doi.org/10.1038/s41586-018-0264-2

Annen C (2011) Implications of incremental emplacement of magma bodies for magma differentiation, thermal aureole dimensions and plutonism–volcanism relationships. Tectonophysics 500(1–4):3–10. https://doi.org/10.1016/j.tecto.2009.04.010

Atherton MP, Sanderson LM (1987) The Cordillera Blanca Batholith; a study of granite intrusion and the relation of cruystal thickening to peraluminosity. Geol Rundsch 76(1):213–232

Bachl CA, Miller CF, Miller JS, Faulds JE (2001) Construction of a pluton; evidence from an exposed cross section of the Searchlight Pluton, Eldorado Mountains, Nevada. Geol Soc Am Bull 113:1213–1228

Barnes CG, Burton BR, Burling TC, Wright JE, Karlsson HR (2001) Petrology and geochemistry of the Late Eocene Harrison Pass Pluton, Ruby Mountains Core Complex, Northeastern Nevada. J Petrol 42:901–930

Bartley JM, Glazner AF, Coleman DS (2018) Dike intrusion and deformation during growth of the Half Dome pluton, Yosemite National Park, California. Geosphere. https://doi.org/10.1130/ges01458.1

Bateman PC (1992) Plutonism in the central part of the Sierra Nevada batholith. California US Geological Survey Professional Paper 1483:186

Bateman PC, Chappell BW (1979) Crystallization, fractionation, and solidification of the Tuolumne intrusive series, Yosemite National Park, California. Geol Soc Am Bull 90:465–482

Bateman PC, Kistler RW, Peck DL, Busacca AJ (1983) Geologic map of the Tuolumne Meadows Quadrangle, Yosemite National Park, California. US Geological Survey Map GQ-1570, scale 1:62,500

Blake DH, Elwell RWD, Gibson IL, Skelhorn RR, Walker GPL (1965) Some relationships resulting from the intimate association of acid and basic magmas. J Geol Soc London 121:31–49

Blundy J, Ulmer P (2006) Evolution of a granite batholith: the Adamello massif, Italian Alps: Troisieme Cycle field workshop, August 28 to September 6, 2006. Dept. of Earth Sciences, Univ. of Bristol

Boudreau A (2011) The evolution of texture and layering in layered intrusions. Int Geol Rev 53:330–353. https://doi.org/10.1080/00206814.2010.496163

Bowen NL (1928) The evolution of the igneous rocks. Princeton University Press, Princeton, New Jersey

Cabane H, Laporte D, Provost A (2005) An experimental study of Ostwald ripening of olivine and plagioclase in silicate melts; implications for the growth and size of crystals in magmas. Contrib Mineral Petrol 150:37–53. https://doi.org/10.1007/s00410-005-0002-2

Cann JR (1970) Upward movement of granitic magma. Geol Mag 107:335–340

Carmichael ISE (1963) The crystallization of feldspar in volcanic acid liquids. J Geol Soc Lond 119(1):95–131
Chappell BH (1996) Magma mixing and the production of compositional variation within granite suites; evidence from the granites of southeastern Australia. J Petrol 37(3):449–470
Clarke DB (2007) Assimilation of xenocrysts in granitic magmas: principles, processes, proxies, and problems. Can Mineral 45:5–30
Clemens JD, Stevens G (2012) What controls chemical variation in granitic magmas? Lithos 134–135:317–329. https://doi.org/10.1016/j.lithos.2012.01.001
Coleman DS, Bartley JM, Glazner AF, Law RD (2005) Incremental assembly and emplacement of Mesozoic Plutons in the Sierra Nevada and White and Inyo Ranges. Geological Society of America Field Forum Field Trip Guide, California. https://doi.org/10.1130/2005.IAAEOM.FFG
Coleman DS, Bartley JM, Glazner AF, Pardue MJ (2012) Is chemical zonation in plutonic rocks driven by changes in source magma composition or shallow-crustal differentiation? Geosphere 8(6):1568–1587. https://doi.org/10.1130/GES00798.1
Coleman DS, Gray W, Glazner AF (2004) Rethinking the emplacement and evolution of zoned plutons: geochronologic evidence for incremental assembly of the Tuolumne Intrusive Suite, California. Geology 32:433–436
Davis JW, Coleman DS, Gracely JT, Gaschnig R, Stearns M (2012) Magma accumulation rates and thermal histories of plutons of the Sierra Nevada Batholith. CA Contrib Mineral Petrol 163(3):449–465. https://doi.org/10.1007/s00410-011-0683-7
Donhowe DP, Hartel RW (1996) Recrystallization of ice cream during controlled accelerated storage. Int Dairy J 6:1191–1208
Eichelberger JC, Izbekov PE, Browne BL (2006) Bulk chemical trends at arc volcanoes are not liquid lines of descent. Lithos 87:135–154. https://doi.org/10.1016/j.lithos.2005.05.006
Erdmann M, Koepke J (2016) Experimental temperature cycling as a powerful tool to enlarge melt pools and crystals at magma storage conditions. Am Mineral 101:960–969. https://doi.org/10.2138/am-2016-5398
Fournier RB (1968) Mechanisms of formation of alaskite, aplite, and pegmatite in a dike swarm, Yosemite National Park, California. In: Coats, RR, Hay, RL, Anderson, CA (eds) Studies in volcanology—a memoir in honor of Howell Williams. Geological Society of America Memoir 116:249–274
Glazner AF (2019) K-feldspar and cooties; or why K-feldspar likes to grow into big crystals. Geological Society of America Abstracts with Programs 51: Abstract 136–13. https://doi.org/10.1130/abs/2019AM-337069
Glazner AF, Bartley JM, Coleman DS, Gray W, Taylor RZ (2004) Are plutons assembled over millions of years by amalgamation from small magma chambers? GSA Today 14(4/5):4–11
Glazner AF, Bartley JM, Law B, Coleman DS (2011) The granite aqueduct and advection of water and heat through plutonic terranes. American Geophysical Union Fall Meeting 2011: Abstract V14B-05
Glazner AF, Bartley JM, Putnam RL, and Stock GM (2018) The shape of Half Dome: 3D studies of morphology and diking. Geological Society of America Abstracts with Programs 50: Abstract 36–3. https://doi.org/10.1130/abs/2018RM-313861
Glazner AF, Coleman DS, Bartley JM (2008) The tenuous connection between high-silica rhyolites and granodiorite plutons. Geology 36(2):183–186. https://doi.org/10.1130/g24496a.1
Glazner AF, Coleman DS, Mills RD (2015) The volcanic-plutonic connection. In: Breitkreuz C, Rocchi S (eds) Physical geology of shallow magmatic systems: dykes, sills, and laccoliths. Springer International Publishing, New York
Glazner AF, Johnson BR (2013) Late crystallization of K-feldspar and the paradox of megacrystic granites. Cont Mineral Petrol 166(3):777–799. https://doi.org/10.1007/s00410-013-0914-1
Gray W, Glazner AF, Coleman DS, Bartley JM (2008) Long-term geochemical variability of the Late Cretaceous Tuolumne Intrusive Suite, central Sierra Nevada, California. Geol Soc Lond Spec Publ 304:183–201
Grove TL, Brown SM (2018) Magmatic processes leading to compositional diversity in igneous rocks: Bowen (1928) revisited. Am J Sci 318:1–28. https://doi.org/10.2475/01.2018.02
Hibbard MJ, Watters RJ (1985) Fracturing and diking in incompletely crystallized granitic plutons. Lithos 18(1):1–12
Hildreth W (2004) Volcanological perspectives on Long Valley, Mammoth Mountain, and Mono Craters: several contiguous but discrete systems. J Volc Geothermal Res 136(3–4):169–198
Holness MB, Vernon, RH (2015) The influence of interfacial energies on igneous microstructures. In: Charlier B, Namur O, Latypov R, Tegner C (eds) Layered intrusions, Springer Geology. Springer, Dordrecht. https://doi.org/10.1007/978-94-017-9652-1_4
Holness MB, Clemens JD, Vernon RH (2018) How deceptive are microstructures in granitic rocks? Answers from integrated physical theory, phase equilibrium, and direct observations. Contrib Mineral Petrol 173:62. https://doi.org/10.1007/s00410-018-1488-8
Hövelmann J, Putnis A, Geisler T, Burkhard CS, Golla-Schindler U (2010) The replacement of plagioclase feldspars by albite : observations from hydrothermal experiments. Contrib Mineral Petrol 159(1):43–59. https://doi.org/10.1007/s00410-009-0415-4
Keller CB, Schoene B, Barboni M, Samperton KM, Husson JM (2015) Volcanic-plutonic parity and the differentiation of the continental crust. Nature 523:301–307. https://doi.org/10.1038/nature14584
Kistler RW (1973) Geologic map of the Hetch Hetchy Reservoir quadrangle, Yosemite National Park, California. U.S. Geological Survey Map GQ-1112, scale 1:62,500.
London D, Hunt LE, Schwing CR, Guttery BM (2020) Feldspar thermometry in pegmatites: truth and consequences. Contrib Mineral Petrol. https://doi.org/10.1007/s00410-019-1617-z
Maughan LL, Christiansen EH, Best MG, Gromme CS, Deino AL, Tingey DG (2002) The Oligocene Lund Tuff, Great Basin, USA; a very large volume monotonous intermediate. J Volcanol Geoth Res 113:129–157
Memeti V, Paterson S, Matzel J, Mundil R, Okaya D (2010) Magmatic lobes as "snapshots" of magma chamber growth and evolution in large, composite batholiths: an example from the Tuolumne intrusion, Sierra Nevada. Calif Geol Soc Am Bull 122(11–12):1912–1931. https://doi.org/10.1130/b30004.1
Michael PJ (1984) Chemical differentiation of the Cordillera Paine granite (southern Chile) by in situ fractional crystallization. Contrib Mineral Petrol 87:179–195
Mills RD, Glazner AF (2013) Experimental study on the effects of temperature cycling on coarsening of plagioclase and olivine in an alkali basalt. Contrib Mineral Petrol 166(1):97–111. https://doi.org/10.1007/s00410-013-0867-4
Mills RD, Ratner JJ, Glazner AF (2011) Experimental evidence for crystal coarsening and fabric development during temperature cycling. Geology. https://doi.org/10.1130/G32394.1
Mustart DA, Horrigan MJ (2000) Hydrothermal pipes in three granitic plutons of the Tuolumne Intrusive Suite, Sierra Nevada Batholith, California. Geol Soc Am Abstr Prog 32(6):52
Niedermeier DRD, Putnis A, Geisler T et al (2009) The mechanism of cation and oxygen isotope exchange in alkali feldspars under hydrothermal conditions. Contrib Mineral Petrol 157:65–76. https://doi.org/10.1007/s00410-008-0320-2
O'Neil JR, Taylor HP Jr (1967) The oxygen isotope and cation exchange chemistry of feldspars. Am Mineral 52:1414–1437
Peng CCJ (1970) Intergranular albite in some granites and syenites of Hong Kong. Am Mineral 55:270–282
Pitcher WS (1993) The nature and origin of granite. Chapman & Hall, London

Putirka KD, Tepley FJ III (2008) Thermometers and barometers for volcanic systems. Rev Mineral Geochem 69:61–120

Putnam R, Glazner AF, Coleman DS, Kylander-Clark ARC, Pavelsky T, Abbot MI (2015) Plutonism in three dimensions; field and geochemical relations on the souheast face of El Capitan, Yosemite National park. Calif Geosphere 11(4):1133–1157. https://doi.org/10.1130/GES01133.1

Putnis A (2002) Mineral replacement reactions; from macroscopic observations to microscopic mechanisms. Mineral Mag 66(5):689–708

Rogers JJW (1961) Origin of albite in granitic rocks. Am J Sci 259:186–193

Ruiz-Agudo E, Putnis CV, Putnis A (2014) Coupled dissolution and precipitation at mineral–fluid interfaces. Chem Geol 383:132–146. https://doi.org/10.1016/j.chemgeo.2014.06.007

Sisson TW, Grove TL, Coleman DS (1996) Hornblende gabbro sill complex at Onion Valley, California, and a mixing origin for the Sierra Nevada Batholith. Contrib Mineral Petrol 126(1–2):81–108. https://doi.org/10.1007/s004100050237

Sisson TW, Ratajeski K, Hankins WB, Glazner AF (2005) Voluminous granitic magmas from common basaltic sources. Contrib Mineral Petrol 148(6):635–661

Stephens WE, Halliday AN (1980) Discontinuities in the composition surface of a zoned pluton, Criffell, Scotland. Geol Soc Am Bull Part I 91:165–170

Stevens G, Villaros A, Moyen J-F (2007) Selective peritectic garnet entrainment as the origin of geochemical diversity in S-type granites. Geology 35(1):9–12. https://doi.org/10.1130/G22959A.1

Valley JW, Graham CM (1996) Ion microprobe analysis of oxygen isotope ratios in quartz from Skye granite: healed micro-cracks, fluid flow, and hydrothermal exchange. Contrib Mineral Petrol 124:225–234

White AJR, Chappell BW (1977) Ultrametamorphism and granitoid genesis. Tectonophysics 43:7–22

Zorpi MJ, Coulon C, Orsini JB, Cocirta C (1989) Magma mingling, zoning and emplacement in calc-alkaline granitoid plutons. Tectonophysics 157:315–329